Ratio of positron to electron bremsstrahlung energy loss: An approximate scaling law

Longhuan Kim and R. H. Pratt
Department of Physics and Astronomy, University of Pittsburgh, Pittsburgh, Pennsylvania 15260

S. M. Seltzer and M. J. Berger
Center for Radiation Research, National Bureau of Standards, Washington, D.C. 20234
(Received 18 November 1985)

We have calculated the total energy loss of an incident electron or positron due to the bremsstrahlung radiation from various atoms during a scattering. The kinetic energies considered for the incident electrons and positrons were 10, 50, and 500 keV. The calculations were performed with our relativistic partial-wave multipole-expansion numerical code [H. K. Tseng and R. H. Pratt, Phys. Rev. A 3, 100 (1971)]. The differences between the radiative energy loss of positrons and electrons are considerable and cannot be disregarded. We observe that the ratio of the radiative energy loss for positrons to that for electrons obeys a simple scaling law, being expressible fairly accurately as a function only of the quantity T_1/Z^2, where T_1 is the incident-particle kinetic energy and Z is the atomic number of the scatterer. This scaling law makes it possible to obtain the energy loss for positrons from existing electron bremsstrahlung data. The scaling is exact in the case of the point Coulomb potential, both in the classical bremsstrahlung formula and the nonrelativistic dipole Sommerfeld formula, not only for the ratio of total energy losses but also for the separate energy losses and even for the radiation energy spectrum. In the screened case scaling is significantly broken for the spectrum and for the total energy loss but remains fairly good for the ratio of the total energy losses. We will discuss scaling features of bremsstrahlung radiation energy loss and the behavior for both high and low energies.

I. INTRODUCTION

In this paper we wish to report a study of the scaling properties of positron and electron bremsstrahlung energy loss, considered as a function of the kinetic energy T_1 of the projectile and the charge Z of the scatterer. When a charged particle traverses an atomic field some of its kinetic energy is converted into photon energy of bremsstrahlung radiation. This radiation energy loss is of interest, for example, in high-temperature plasma physics, where it is a major cause of energy loss from plasmas. A characterization of this loss is provided by the radiative stopping power, defined as the mean energy loss per unit pathlength due to bremsstrahlung radiation. The stopping power is useful, for example, in estimating the fraction of beam energy converted into bremsstrahlung energy when a beam of particles traverses a thick target. The radiative stopping power for a given elemental target and type of beam particle can be obtained from the integrated energy loss cross section $\Phi_{\rm rad}$, which in turn is obtained by integrating the singly differential energy spectrum $k(d\sigma/dk)$ for bremsstrahlung radiation in the scattering of a particle from the target over the photon energy spectrum:

$$\Phi_{\rm rad}=\frac{1}{Z_2\alpha_3(T_1+E_0)}\int_0^{T_1}k\frac{d\sigma}{dk}dk\,, \tag{1}$$

where k is the photon energy, T_1 is the kinetic energy of beam particle, Z is the atomic number of target element, E_0 is the rest energy of the beam particle, and α is the fine-structure constant. The natural units (i.e., $\hbar=m_e=c=1$) are used throughout this paper unless explicitly specified otherwise.

Various methods are available to calculate the bremsstrahlung radiation energy spectrum. The present state of the art is represented by the relativistic partial-wave numerical calculations carried out by Tseng and Pratt.[1] Tables of results interpolated from such calculations for $2\leqq Z\leqq 92$, $1\leqq T_1\leqq 500$ keV have been published.[2] Some data for positron bremsstrahlung utilizing the same type of calculation are also available.[3] In a recent stopping power tabulation,[4] these results were used to obtain the radiative stopping power for electrons and positrons. The differences between the radiative stopping powers of positrons and electrons are considerable and cannot be disregarded. Note that the simple Born approximation without Elwert factor (a Coulomb correction) does not distinguish electron and positron bremsstrahlung. Reference 3 provided results only for a few situations (at 10, 50, and 500 keV for $Z=8$ and 92). Such numerical cross-section calculations are expensive and cannot readily be extended to all the many situations of interest. However, it was noticed in Ref. 4 that the ratio of the radiative stopping power for positrons to that for electrons,

$$\eta(T_1,Z)=\frac{\Phi^+_{\rm rad}(T_1,Z)}{\Phi^-_{\rm rad}(T_1,Z)}\,, \tag{2}$$

where $\pm$ corresponds to the positron (electron) case, obeys a simple scaling law, being expressible fairly accurately as a function only of the quantity T_1/Z^2 [i.e., η

$=\eta(T_1/Z^2)]$.

This scaling feature has encouraged us to make a systematic study of the scaling properties of bremsstrahlung cross sections. To some extent, scaling features exist not only in the ratios of the energy losses but also in the separate energy loss cross sections and also in the bremsstrahlung spectra themselves. In both the classical and the nonrelativistic quantum-mechanical dipole approximations, scaling can be demonstrated analytically as an exact feature in the point Coulomb potential at all levels (the spectrum, the energy loss and the positron-to-electron ratio of energy losses). In the screened case, the scaling features are significantly broken at the spectrum level and the energy-loss level, but remain fairly good for ratio of the energy loss. The quantitative nature of the function η (ratio of the energy loss versus T_1/Z^2) depends on the approximations used. However, in the limiting cases (both high energy and low energy), the asymptotic behavior of η function calculated from various approximations is similar.

We begin, in Sec. II, with a description of the method of calculation of the bremsstrahlung spectrum which we employ in this work, and with the results obtained in this way for both Coulomb and screened potential cases. This is followed by a discussion of scaling features of the spectrum. In Sec. III we present our results for the integrated energy loss for electron and positron bremsstrahlung and for the ratio of these energy losses. We discuss the scaling features of these quantities and the causes for variations in these features. The asymptotic behavior of the energy-loss ratio $\eta(T_1/Z^2)$ at both high energy and low energy is discussed in this section. Finally, an example of application of the scaling law is given in Sec. IV.

II. SCALING PROPERTIES OF RADIATION SPECTRUM OF POSITRON AND ELECTRON BREMSSTRAHLUNG

The bremsstrahlung spectrum is often tabulated in the scaled form

$$\sigma=(\beta_1^2/Z^2)k\,d\sigma/dk\,, \tag{3}$$

where β_1 is the velocity of the incident particle in units of velocity of light, Z is the atomic number of the target atom, and $d\sigma/dk$ is the bremsstrahlung cross-section differential in emitted photon energy k (integrated over angles).

For a given type of potential, σ is a function of k, T_1, and Z. With the point Coulomb potential, analytic expressions for $\sigma(k,T_1,Z)$ are obtained both in classical and in nonrelativistic quantum theory. The classical formula for the point Coulomb potential (CC),[5] which was originally derived by Kramers (though his name is usually associated with the limiting cases) is

$$\sigma_{\rm CC}^{-}(k,T_1,Z)=(4\pi^2\alpha^3/3)i\mu H_{i\mu}^{(1)}(i\mu)H_{i\mu}^{(1)'}(i\mu) \tag{4}$$

for electron bremsstrahlung and

$$\sigma_{\rm CC}^{+}(k,T_1,Z)=e^{-2\pi\mu}\sigma_{\rm CC}^{-}(k,T_1,Z) \tag{5}$$

for positron bremsstrahlung, with

$$\mu=\tfrac{1}{2}\nu_1 k/T_1=2^{-3/2}\alpha(k/T_1)(Z^2/T_1)^{1/2}, \tag{6}$$

where $H^{(1)}$ and $H^{(1)'}$ are the Hankel function and its derivative, respectively.

The Sommerfeld formula[6] for the spectrum according to nonrelativistic quantum mechanics in dipole approximation (S) is

$$\sigma_S^{\pm}(k,T_1,Z)=\frac{16\pi^2\alpha^3}{3}\frac{1}{(e^{\mp\pi\nu_1}-1)(1-e^{\pm 2\pi\nu_2})}\times X_0\frac{d}{dX_0}\,|F(i\nu_1,i\nu_2;X_0)|^2, \tag{7}$$

with

$$\nu_1=Z\alpha/\beta_1=2^{-1/2}\alpha(Z^2/T_1)^{1/2}, \tag{8}$$

$$\nu_2=Z\alpha/\beta_2=\nu_1/(1-k/T_1)^{1/2}, \tag{9}$$

$$X_0=-4\nu_1\nu_2/(\nu_1-\nu_2)^2\,. \tag{10}$$

Tables for numerical evaluation of these formulas have been given, for instance, by Florescu and Costescu,[7] extending earlier tabulations.

For neutral atoms where bound electrons screen the Coulomb nuclear charge, we use numerical approaches. Our fully relativistic partial-wave multipole independent-particle approximation code calculates free-free transition cross sections for electrons or positrons in a self-consistent Dirac-Slater potential (no Latter tail is used). The calculations provide our most accurate results for screened potentials ("exact" screened results, ES) compared to other simpler methods. This code can also be applied to obtain relativistic predictions in the point Coulomb potential ("exact" Coulomb results, EC), though, often, excessive computer time is required. Table I gives numerically calculated values of σ^+,σ^- and of the ratio σ^+/σ^- for the six combinations of T_1 and Z treated by Feng *et al.*[3] and also for eight additional combinations which we have now obtained. The ES calculations in the soft photon region of a spectrum are more difficult than in other regions due to the involvement of a large number of partial waves. In the extreme case of the soft photon end point ($k=0$) we may use elastic scattering theory and the low-energy theorem. Also, our code was not designed to handle the zero-energy outgoing electrons which occur at the hard photon end point of the spectrum. For these reasons our tables include values in parentheses which are interpolated or extrapolated.

Numerical calculations of classical bremsstrahlung in screened potentials have not been available. Recently, we have developed a computer code which calculates the classical bremsstrahlung doubly differential cross sections, both for the Coulomb potential and for screened potentials.[8] The code calculates numerically the trajectory of an incident electron (or positron) in a central potential according to classical dynamics, then calculates the dipole radiation emitted on the trajectory, and integrates over all the trajectories in the incident beam of particles. A Fourier transform of the time dependence of the radiated energy gives its spectrum. It is assumed that the loss of kinetic energy of the incident electron due to the radiation

TABLE I. Positron (+) and electron (−) bremsstrahlung spectra and their ratio calculated with the relativistic partial-wave multipole expansion numerical method, as function of the fraction k/T_1 of incident energy radiated. Values in parentheses are interpolated or extrapolated. The last column gives the corresponding results for the integrated radiative energy-loss cross section Φ_{rad}. Negative numbers in parentheses indicate powers of 10.

Z	T_1 (keV)		$(\beta_1^2/Z^2)\,k d\sigma^{\pm}/dk$ (mb) $k/T_1=0$	0.2	0.4	0.6	0.8	0.9	1.0	Φ_{rad}
2	10	(+)	9.59	(7.74)	5.76	3.91	2.15	1.17	0	4.26
		(−)	10.45	(8.55)	6.66	5.10	3.71	2.97	(2.13)	5.28
		(+)/(−)	0.918	0.905	0.865	0.767	0.580	0.394	0	0.807
2	500	(+)	14.0	(7.26)	4.23	2.79	1.56	0.953	0	5.11
		(−)	14.0	(7.16)	4.34	2.91	1.68	1.08	(0.454)	5.19
		(+)/(−)	1.00	0.986	0.975	0.959	0.929	0.882	0	0.985
8	10	(+)	7.33	(5.46)	(3.74)	2.24	0.789	0.237	0	2.75
		(−)	8.39	(7.91)	7.03	6.14	5.45	5.22	(5.08)	5.80
		(+)/(−)	0.874	0.690	0.532	0.365	0.145	4.54(−2)	0	0.474
8	50	(+)	9.86	7.20	4.94	3.14	1.48	0.652	0	3.89
		(−)	10.5	(8.25)	6.43	5.01	3.86	3.33	(2.80)	5.44
		(+)/(−)	0.939	0.873	0.768	0.627	0.383	0.196	0	0.715
8	500	(+)	12.2	6.95	4.38	2.68	1.39	0.776	0	4.81
		(−)	12.6	(7.31)	(4.74)	3.04	1.86	1.29	(0.644)	5.27
		(+)/(−)	0.968	0.951	0.924	0.882	0.747	0.602	0	0.913
13	10	(+)	6.33	(4.97)	3.10	1.45	0.352	7.34(−2)	0	2.26
		(−)	7.80	(7.39)	6.77	6.21	5.79	5.62	(5.46)	5.72
		(+)/(−)	0.812	0.673	0.458	0.233	6.08(−2)	1.31(−2)	0	0.395
13	500	(+)	11.8	(6.67)	4.15	2.52	1.25	0.646	0	4.58
		(−)	12.3	(7.35)	4.93	3.29	2.03	1.47	(0.931)	5.42
		(+)/(−)	0.959	0.907	0.842	0.766	0.616	0.439	0	0.845
29	10	(+)	4.49	(3.02)	1.45	0.454	5.38(−2)	5.53(−3)	0	1.25
		(−)	6.08	(6.08)	5.89	5.67	5.48	5.40	(5.33)	5.03
		(+)/(−)	0.738	0.497	0.246	8.01(−2)	9.82(−3)	1.02(−3)	0	0.249
29	500	(+)	10.7	(6.20)	3.67	2.09	0.874	0.441	0	4.08
		(−)	11.6	(7.60)	5.31	3.74	2.54	2.04	(1.60)	5.83
		(+)/(−)	0.922	0.816	0.691	0.559	0.344	0.216	0	0.700
47	10	(+)	3.06	(1.92)	0.778	0.187	1.35(−2)	9.19(−4)	0	0.761
		(−)	4.81	(4.92)	5.00	5.02	4.99	4.97	(4.96)	4.32
		(+)/(−)	0.636	0.390	0.156	3.73(−2)	2.71(−3)	1.85(−4)	0	0.176
47	500	(+)	9.72	(5.82)	3.21	1.70	0.575	0.163	0	3.63
		(−)	11.4	(7.84)	5.73	4.24	3.10	2.64	(2.25)	6.28
		(+)/(−)	0.853	0.742	0.560	0.401	0.185	6.17(−2)	0	0.578
92	10	(+)	1.54	(0.757)	0.274	4.48(−2)	1.79(−3)	7.13(−5)	0	0.306
		(−)	3.04	(3.36)	3.63	3.84	3.99	4.04	(4.07)	3.21
		(+)/(−)	0.507	0.225	7.55(−2)	1.17(−2)	4.49(−4)	1.76(−5)	0	9.53(−2)
92	50	(+)	4.25	2.42	0.847	0.167	8.33(−3)	3.37(−4)	0	0.978
		(−)	6.67	(6.49)	6.18	5.91	5.72	5.64	(5.56)	5.50
		(+)/(−)	0.637	0.373	0.137	2.83(−2)	1.46(−3)	5.98(−5)	0	0.178
92	500	(+)	7.87	4.44	2.34	1.01	0.208	2.89(−2)	0	2.65
		(−)	11.7	(8.56)	6.56	5.16	4.35	3.99	(3.55)	7.33
		(+)/(−)	0.672	0.519	0.357	0.196	4.78(−2)	7.24(−3)	0	0.362

is negligible and does not affect the orbit. Retardation effects are also neglected.

One can observe from Eqs. (4)–(10) that in the Coulomb case, for a fixed value of k/T_1, both the classical and the nonrelativistic quantum-mechanical dipole bremsstrahlung cross section are dependent on T_1/Z^2 only. In a screened potential, generally, the spectrum depends not only on T_1/Z^2 but also on further properties of the given potential and T_1. For example, consider a potential described as $V=-(Ze^2/r)g(\lambda r)$, where $g(\lambda r)$ is a screening function and λ is a screening parameter, with $g(0)=1$. From classical electromagnetic theory[5] the photon-energy spectrum during a bremsstrahlung scattering is

$$k\frac{d\sigma}{dk}=\frac{16\pi^2}{3}\int_0^\infty |\ddot{d}_k|^2 b\,db\,, \tag{11}$$

where $\ddot{d}_k$ is the Fourier transform of the second time derivative of the dipole moment of the scattering system and b is the impact parameter. In the central potential which we consider

$$|\ddot{d}_k|^2=\alpha\left|\int_{-\infty}^{+\infty}-\nabla_r\left[\frac{Z\alpha}{r}g(\lambda r)\right]e^{ikt}dt\right|^2, \tag{12}$$

$$r=r(T_1,b,t)\,. \tag{13}$$

Introducing new variables

$$\rho=\frac{r}{b},\quad \Lambda=\lambda b,\quad \tau=\frac{a^{1/2}}{b^{3/2}}t,\quad \epsilon=\frac{b}{a}T_1,\quad a=Z\alpha\,, \tag{14}$$

Eq. (11) can be rewritten as

$$k\frac{d\sigma}{dk}=\frac{16\pi^2}{3}\alpha a\int_0^{+\infty}\left|\int_{-\infty}^{+\infty}-\nabla_\rho\left[\frac{1}{\rho}g(\Lambda\rho)\right]\exp(ikb^{3/2}\tau/a^{1/2})d\tau\right|^2 db\,. \tag{15}$$

Since $b=a\epsilon/T_1$ and $db=(a/T_1)d\epsilon$,

$$k\frac{d\sigma}{dk}=\frac{16\pi^2\alpha a^2}{3T_1}\int_0^{+\infty}\left|\int_{-\infty}^{+\infty}-\nabla_\rho\left[\frac{1}{\rho}g(\Lambda\rho)\right]\exp(ika\epsilon^{3/2}\tau/T_1^{3/2})d\tau\right|^2 d\epsilon\,, \tag{16}$$

or

$$\sigma=\frac{32\pi^2\alpha^3}{3}\int_0^{+\infty}\left|\int_{-\infty}^{+\infty}-\nabla_\rho\left[\frac{1}{\rho}g(\Lambda\rho)\right]\exp(ika\epsilon^{3/2}\tau/T_1^{3/2})d\tau\right|^2 d\epsilon\,, \tag{17}$$

with $\rho=\rho(\Lambda,\epsilon,\tau)$; i.e.,

$$\sigma=\sigma(ka/T_1^{3/2},\Lambda)=\sigma(\mu,\lambda Z/T_1)\,. \tag{18}$$

We see that in this case the classical bremsstrahlung cross section is a function of two parameters μ and $Z\lambda/T_1$, rather than the single parameter μ of the point Coulomb case. The radiation spectrum does not scale with T_1/Z^2, unless either the dependence of the cross section on the second parameter is weak or λ is directly proportional to Z. One could better satisfy such requirements by considering a more restricted range of elements (for instance, omitting the low-Z cases).

In Fig. 1 we compare the scaling features of the classical bremsstrahlung spectrum from the point Coulomb potential with the classical results in the screened case, for the choice of energy-loss ratio $k/T_1=0.2$ as an example. The solid line refers to the point Coulomb case, where the spectrum for given value of k/T_1 ($=0.2$ in this example) is determined only by T_1/Z^2, while in the screened case (shown by the data points marked with symbols) the spectrum depends not only on T_1/Z^2 but also on Z. We see the data points are spread out and can not be fitted by a single smooth curve. In the region where T_1/Z^2 is large the screened results are close to the point Coulomb results, since screening effects are relatively small for high-energy incident electrons.

The scaling feature of the classical Coulomb bremsstrahlung shown above also applies to the positron case

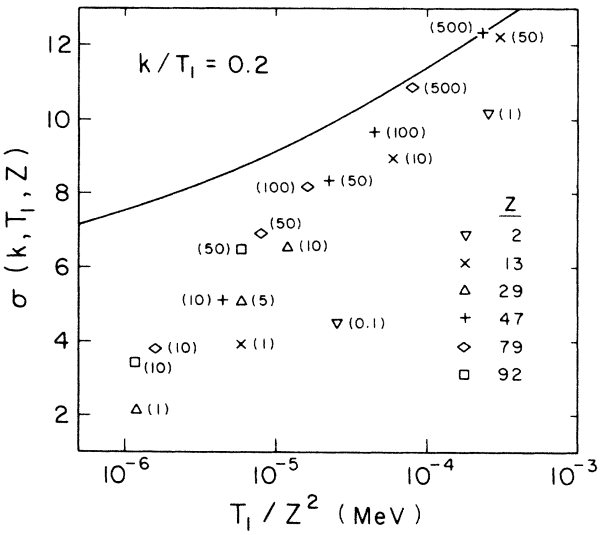

FIG. 1. Scaling of the classical bremsstrahlung spectrum in the point Coulomb case compared with the screened case for the energy-loss ratio $k/T_1=0.2$. The solid line refers to the point Coulomb case, indicating an exact scaling of the spectrum with T_1/Z^2. The discrete points marked with symbols refer to the screened case, showing the dependence of the spectrum on both T_1/Z^2 and Z. Numbers in parentheses indicate the incident kinetic energy in keV.

since the spectrum for positrons differs from that for electrons only by the factor given in Eq. (5). We show in Fig. 2, for the case of Al at 10 keV, a comparison of the positron and electron spectra according to the classical method, the Sommerfeld formula, and the partial-wave calculation, using the Dirac-Slater self-consistent potential for the screened case. The difference between electron and positron bremsstrahlung spectra can be characterized by the ratio of the cross sections $R(k,T_1,Z)=\sigma^+/\sigma^-$. In the classical case for the point Coulomb potential this ratio is

$$R_C=e^{-2\pi\mu}, \tag{19}$$

$$\mu=\frac{Z\alpha}{2\beta_1}\left[\frac{k}{T_1}\right]. \tag{20}$$

$R_C=1$ at the soft photon end point ($k/T_1=0$) and goes to a finite value when $k/T_1\rightarrow 1$; the finite value is zero in the limit of low incident energies and approaches 1 (i.e., a constant ratio across the spectrum) as T_1/Z^2 becomes large. The Sommerfeld result for the ratio of the cross sections is

$$R_S=\exp[-2\pi(\nu_2-\nu_1)]. \tag{21}$$

Like R_C, $R_S=1$ at the soft photon end point (where $\nu_2=\nu_1$), but for all incident energies $R_S=0$ at the tip of the spectrum where $k/T_1\rightarrow 1$ and $\nu_2\rightarrow\infty$. To see the difference between R_C and R_S more clearly we rewrite μ and $\nu_2-\nu_1$ in terms of β_1 and β_2:

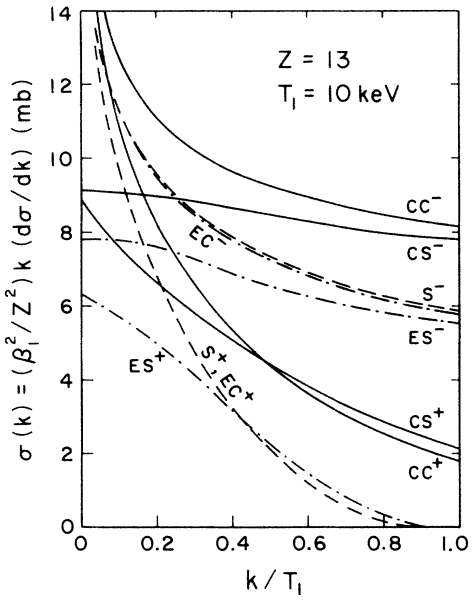

FIG. 2. Comparison of electron and positron bremsstrahlung spectra for Al at 10 keV. CC, classical with Coulomb potential; CS, classical method with Dirac-Slater potential; S, Sommerfeld's method; ES, exact quantum-mechanical partial-wave method with Dirac-Slater potential; EC, exact quantum-mechanical partial-wave method with Coulomb potential; the + and − signs represent positron and electron cases, respectively.

$$\mu=\tfrac{1}{2}Z\alpha(\beta_1^2-\beta_2^2)/\beta_1^3, \tag{22}$$

$$\nu_2-\nu_1=Z\alpha(1/\beta_2-1/\beta_1). \tag{23}$$

Then

$$(\nu_2-\nu_1)/\mu=2(\beta_1/\beta_2)/(1+\beta_2/\beta_1)\geq 1, \tag{24}$$

since $\beta_1\geq\beta_2$. So, for all k/T_1, R_S is always smaller than R_C.

For a screened potential both positron and electron cross sections are reduced significantly in the soft photon region (there is no longer a logarithmic divergence of the energy spectrum in the neutral atom case). The positron cross section is lower than the electron cross section, so that $R<1$ even at the soft photon end point where $R=1$ if there is no screening. We will discuss further in Sec. III the consequences of these features for the energy losses and the ratio of energy losses.

III. SCALING PROPERTIES OF THE ENERGY LOSS AND THE RATIO OF ENERGY LOSSES

The energy-loss cross section defined by Eq. (1) can be rewritten in terms of the scaled cross section $\sigma(k/T_1)=(\beta_1^2/Z^2)k(d\sigma/dk)$ as

$$\Phi^{\pm}(T_1,Z)=\frac{T_1}{\alpha^3\beta_1^2(T_1+E_0)}\int_0^1\sigma^{\pm}(k/T_1)d(k/T_1). \tag{25}$$

In the nonrelativistic case

$$\Phi^{\pm}(T_1,Z)=\frac{1}{2\alpha^3}\int_0^1\sigma^{\pm}(K/T_1)d(K/T_1). \tag{26}$$

The ratio is

$$\eta(T_1,Z)=\frac{\int_0^1\sigma^+(k/T_1)d(k/T_1)}{\int_0^1\sigma^-(k/T_1)d(k/T_1)}. \tag{27}$$

In the classical Coulomb formula the cross section depends on a single variable μ which combines k/T_1 and T_1/Z^2 [Eqs. (4)–(6)]. In the Sommerfeld formula the cross section depends on the two variables ν_1 and ν_2, which can be represented by k/T_1 and T_1/Z^2 [Eqs. (7)–(9)]. In both cases the integration over the spectrum (i.e., the total energy loss) results in a function of the single parameter T_1/Z^2. (While the nonrelativistic cross section σ depends only on *two* variables ν_1 and ν_2, the corresponding relativistic σ depends on *three* variables, and consequently the energy loss is a function of *two* variables. However, in Born approximation the cross section simplifies to two variables, the energy loss to one variable.)

In the screened case, generally, exact scaling is broken for the energy loss due to the additional parameters which have been introduced by the screened potential. Figure 3 shows the energy-loss cross sections of positron and electron classical bremsstrahlung in the Dirac-Slater potential, as well as the ratios of the cross sections. The values of $\Phi^+_{\rm rad}$, $\Phi^-_{\rm rad}$, and the ratios $\eta=\Phi^+_{\rm rad}/\Phi^-_{\rm rad}$ for various combinations of T_1 and Z are plotted versus T_1/Z^2. We see that indeed the screened energy-loss cross sections do not exactly scale. However, the ratio of the energy-loss

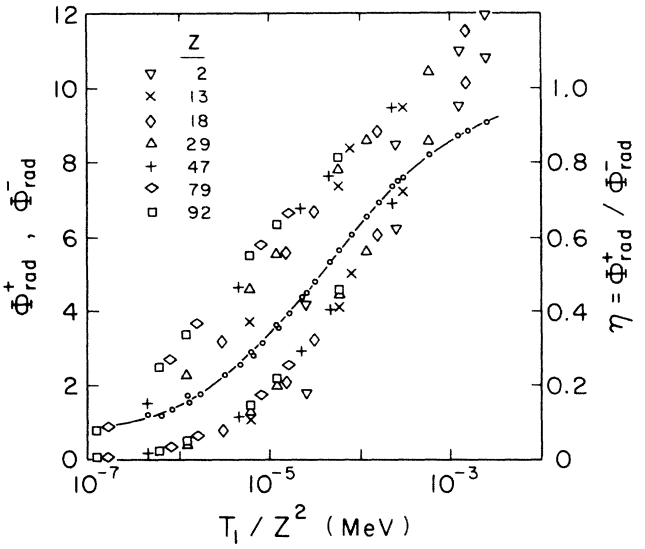

FIG. 3. Energy-loss cross sections of electron and positron bremsstrahlung from neutral atoms and the ratio of the losses [Eq. (27)] calculated from the classical numerical method, as functions of T_1/Z^2. Symbols appear in pairs for a given value of T_1/Z^2. The upper points are for electrons and the lower points are for positrons. The ratios of the two energy losses are marked with small circles and are fitted by a smooth curve.

cross sections does show much better scaling. The ratio $\eta(T_1,Z)$ satisfies scaling to a greater extent than the separate energy losses.

Figure 4 shows the ratios of energy losses from the relativistic partial-wave calculations of the losses, which are given in the last column of Table I. As we see, these data points are close to a single curve, which was obtained by a least-squares fit. The actual shape of the ratio curve η versus T_1/Z^2 varies according to the method with which the spectrum is calculated. To see this, in Fig. 5 we show comparisons of the ratio of positron to electron bremsstrahlung energy-loss cross sections calculated from the classical Coulomb formula (CC), our classical screened numerical calculation (CS), and from the Sommerfeld formula (S), with results from our relativistic partial-wave calculations (EC for the Coulombic case and a fitted ES for the screened case). Deviations from scaling in the CS, EC, and ES cases are neglected. The difference between the classical results (CC) and the Sommerfeld results (S) is due to quantum-mechanical effects, while the difference between the Sommerfeld results and the exact screened results (ES) reflects screening effects, higher multipoles, retardation, and relativity.

In Fig. 5 all curves approach 1 (i.e., equal radiation from electrons and positrons) for large T_1/Z^2 (large incident energy and/or low Z) and approach zero (i.e., relatively little radiation from positrons) when T_1/Z^2 goes to zero (small incident energy and/or high Z). For classical Coulomb and Sommerfeld formulas, as one can see from the asymptotic behavior of the energy-loss ratio, which we will discuss later, these two limits are exact. Considering the spectra of the radiation, one sees from Table I that the positron cross section, while comparable to the electron cross section for soft photon emission $k/T_1 \rightarrow 0$, drops rapidly as k/T_1 increases when T_1/Z^2 is small, resulting in a small value in this case for the ratio of the energy losses. For large T_1/Z^2, the positron cross section differs

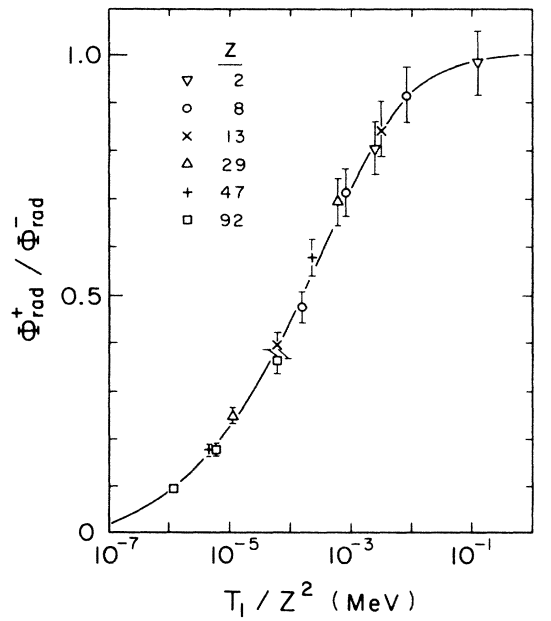

FIG. 4. Ratio $\Phi^+_{rad}/\Phi^-_{rad}$ of positron and electron integrated energy-loss cross sections from neutral atoms as a function of T_1/Z^2, calculated from the relativistic partial-wave multipole expansion.

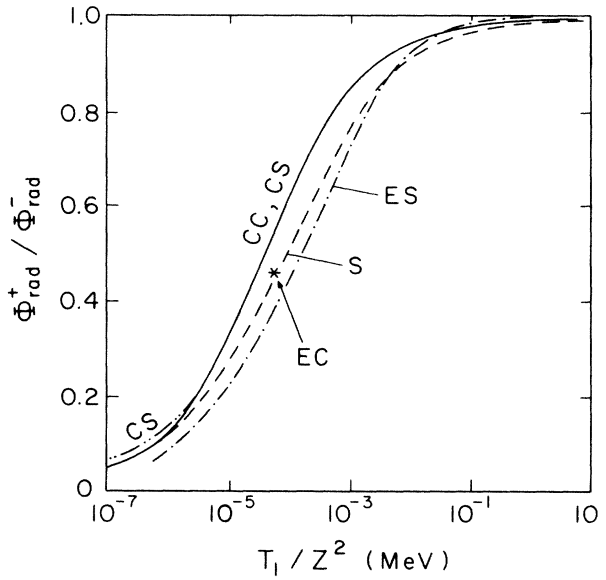

FIG. 5. Comparison of ratios of positron-to-electron integrated energy-loss cross sections calculated from the classical Coulomb formula (CC), classical screened numerical method (CS), Sommerfeld's formula with nonrelativistic kinematics (S), and the relativistic partial-wave expansion method for isolated neutral atoms (ES). The asterisk indicates a single data point we have obtained for totally ionized aluminum for $T_1 = 10$ keV with the relativistic partial-wave multipole expansion.

significantly from the electron cross section only at the hard photon end of the spectrum, so that the ratio of the energy losses is close to 1.

In the classical Coulomb case, the asymptotic behaviors of the curve can be found analytically. Florescu and Costescu[7] have given large and small μ expansion of Eq. (4). The expansion for small μ is

$$\sigma_{CC}=\frac{16\alpha^3}{3}\left[(1+\pi\mu)\ln\left[\frac{2}{\gamma\mu}\right]+O(\mu^2)\right], \tag{28}$$

and the expansion for large μ is

$$\sigma_{CC}=\frac{16\pi\alpha^3}{3^{3/2}}[1+d_1\mu^{-2/3}+d_2\mu^{-4/3}+2d_1d_2\mu^{-2}+O(\mu^{-8/3})], \tag{29}$$

where $d_1=0.217\,747$, $d_2=-0.013\,121\,4$, $\gamma=e^C=1.7807$, and C is the Euler constant. Using Eqs. (5), (28), and (29) we may derive asymptotic analytic forms of the curve $\Phi^+_{rad}/\Phi^-_{rad}$ versus T_1/Z^2 for classical bremsstrahlung. For $T_1/Z^2\to\infty$,

$$\frac{\Phi^+}{\Phi_-}\sim 1-\tfrac{1}{2}\pi\nu_1-\tfrac{1}{4}\pi\nu_1\left[\ln\left[\frac{\gamma\nu_1}{4}\right]\right]^{-1}, \tag{30}$$

and for $T_1/Z^2\to 0$,

$$\frac{\Phi^+}{\Phi^-}\sim C_1\left[\frac{1}{\nu_1}-2^{2/3}d_1\frac{3}{\nu_1^{5/3}}+O(1/\nu_1^{7/3})\right], \tag{31}$$

where

$$C_1=\frac{3^{3/2}}{8\pi\alpha^3}\int_0^\infty\sigma^+_{CC}(\mu)d\mu=\frac{3^{1/2}\pi}{2}\int_0^\infty e^{-2\pi\mu}i\mu H^{(1)}_{i\mu}(i\mu)H^{(1)'}_{i\mu}(i\mu)d\mu\ . \tag{32}$$

The numerical value of C_1 is about 0.57. Equations (30) and (31) are in good agreement with our numerical evaluations.

In screened potentials the situation is more complicated. Screening is important for low-energy incident particles, while for particles of very high energy, which penetrate deeply into the atom during the scattering, the process depends on short distance behavior of the field and the screening of the field by bound electrons is not important. According to our numerical calculations, for classical bremsstrahlung screening changes the spectrum little (except near the soft photon end point) when T_1/Z^2 is greater than 10^{-2} MeV. For T_1/Z^2 between 10^{-5} and 10^{-2} MeV, screening does change both electron and positron cross sections but does not change significantly the ratio of the energy losses. Only when T_1/Z^2 is less than 10^{-5} MeV does the screened ratio become significantly different from the Coulomb ratio (about 10% different by $T_1/Z^2=2\times10^{-6}$ MeV). However, in quantum-mechanical partial-wave calculations the difference occurs much earlier. (It is in fact difficult to do direct EC calculations for the soft photon region of spectrum because of the slow convergence of the numerical procedure, and therefore we do not give detailed comparisons.) From the results of Ref. 3 we find that, for $Z=8$ and $T_1=0.01$ MeV ($T_1/Z^2=1.6\times10^{-4}$ MeV), the Sommerfeld results for the spectrum are in very good agreement with EC results. Therefore, the S curve in Fig. 5 should also represent the EC curve in the vicinity of this point (i.e., $T_1/Z^2=1.6\times10^{-4}$ MeV). We notice that the ES curve at this point is below the S curve by about 10%. The only direct EC numerical result we obtained for Al, $T_1=10$ keV ($T_1/Z^2=0.59\times10^{-4}$ MeV), shown in Fig. 5 by an asterisk, is also in agreement with the S results. Thus, screening in fact does have a significant effect on the quantum ratio in this region.

As already remarked in Sec. II, the positron-to-electron ratio of the spectrum from classical bremsstrahlung, R_C, is always greater than that from the Sommerfeld formula. This explains why in Fig. 5 the S curve is below the CC curve throughout the whole range of T_1/Z^2. In the screened case, the greater suppression of the spectrum in the soft photon region for positrons causes the ES curve to generally lie below both CC and S curves in Fig. 5. (Note however that there is a crossover in Fig. 5, and the hard photon region of the spectrum increases with screening.) Within the energy range which we consider in this work, screening effects on the spectrum become relatively small and negligible (except in the region close to the soft photon end point) when the kinetic energy of the incident particle becomes high. Therefore, in the high-energy region, the ES curve should merge with its Coulomb counterpart. Note that, for high incident energy, the nonrelativistic dipole (Sommerfeld) calculation is not adequate and for large T_1/Z^2 generally overestimates both electron and positron cross sections (see Table II of Ref. 3). It overestimates the cross section for electrons more than it does for positrons, resulting in a slower approach of the ratio to unity.

IV. EXAMPLE OF APPLICATION

Accepting the validity of these approximate scaling features of the ratios of energy losses, it is possible to obtain the radiative stopping power for positrons for all conditions of interest by first estimating positron-electron ratios using the scaling law, and then applying these ratios

TABLE II. Fitted values of the ratios, $\eta=\Phi^+_{rad}/\Phi^-_{rad}$, of the integrated radiative energy-loss cross sections (Table I) for positrons (+) and electrons (−).

T_1/Z^2 (MeV)	$\Phi^+_{rad}/\Phi^-_{rad}$	T_1/Z^2 (MeV)	$\Phi^+_{rad}/\Phi^-_{rad}$
1×10^{-7}	0.020	1×10^{-3}	0.727
2×10^{-7}	0.035	2×10^{-3}	0.802
5×10^{-7}	0.061	5×10^{-3}	0.881
1×10^{-6}	0.088	1×10^{-2}	0.923
2×10^{-6}	0.121	2×10^{-2}	0.952
5×10^{-6}	0.175	5×10^{-2}	0.977
1×10^{-5}	0.225	1×10^{-1}	0.988
2×10^{-5}	0.283	2×10^{-1}	0.996
5×10^{-5}	0.370	5×10^{-1}	1.0
1×10^{-4}	0.446		
2×10^{-4}	0.530		
5×10^{-4}	0.644		

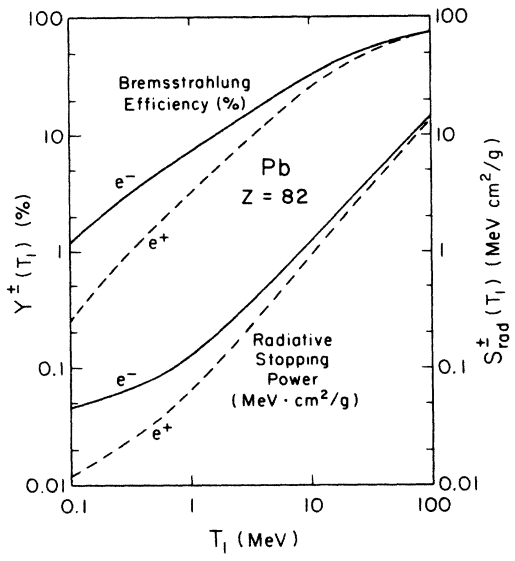

FIG. 6. Positron and electron differences in lead ($Z=82$), for the radiative stopping power, in MeV cm^2/g, and for the bremsstrahlung efficiency, in percent, as a function of the incident particle kinetic energy T_1. Dashed curves are for positrons and solid curves for electrons. The + and − signs represent positron and electron cases, respectively.

to the known radiative stopping powers for electrons.[4,9] The radiative stopping power $S_{\rm rad}$ is defined as the loss of the kinetic energy of an incident particle due to bremsstrahlung radiation per unit path per unit density of the target matter. The fitted values of the ratio curve of Fig. 4 for a logarithmic grid in T_1/Z^2 are given in Table II.[10] As an illustration, we compare in Fig. 6 the electron radiative stopping power $S^-_{\rm rad}$ with that for positrons, $S^+_{\rm rad}$, for the case of lead ($Z=82$). (Note that with the assumption of universal curve, as in Fig. 4, low-energy low-Z data are being utilized to predict high-energy high-Z data.) We also show in Fig. 6 the corresponding results for the bremsstrahlung efficiency $Y^\pm$ (the fraction of incident kinetic energy converted to bremsstrahlung photons as the particle slows down to rest), evaluated as

$$Y^\pm(T_1)=\frac{1}{T_1}\int_0^{T_1}\frac{S^\pm_{\rm rad}(T)}{S^\pm_{\rm col}(T)+S^\pm_{\rm rad}(T)}dT\,, \tag{33}$$

where $S^\pm_{\rm col}$ is the collisional stopping power.[4,11]

ACKNOWLEDGMENTS

This work was supported in part by the National Science Foundation under Grant No. PHY-84-20845, and also by the U.S. Office of Naval Research and the U.S. Department of Energy.

[1]H. K. Tseng and R. H. Pratt, Phys. Rev. A 3, 100 (1971).
[2]R. H. Pratt, H. K. Tseng, C. M. Lee, L. Kissel, C. MacCallum, and M. Riley, At. Data Nucl. Data Tables 20, 175 (1977); 26, 477 (1981), erratum.
[3]I. J. Feng, R. H. Pratt, and H. K. Tseng, Phys. Rev. A 24, 1358 (1981).
[4]M. J. Berger and S. M. Seltzer, Nat. Bur. Stand. (U.S.) Misc. Publ. No. 82-2550-A (U.S. GPO, Washington, D.C., 1982).
[5]L. D. Landau and E. M. Lifshitz, *The Classical Theory of Fields*, 3rd ed. (Pergamon, New York, 1971).
[6]A. Sommerfeld, Ann. Phys. (Leipzig) 11, 257 (1931).
[7]V. Florescu and A. Costescu, Rev. Roum. Phys. 23, 131 (1978); P. Kirkpatrik and L. Wiedmann, Phys. Rev. 67, 321 (1945).
[8]Longhuan Kim and R. H. Pratt (unpublished).
[9]S. M. Seltzer and M. J. Berger, Int. J. Appl. Radiat. Isot. 33, 1219 (1982).
[10]Because of the additional data from the present work, these values are slightly different from those used in Ref. 4.
[11]S. M. Seltzer and M. J. Berger, Int. J. Appl. Radiat. Isot. 33, 1189 (1982).